RSC Advances

This is an *Accepted Manuscript*, which has been through the Royal Society of Chemistry peer review process and has been accepted for publication.

Accepted Manuscripts are published online shortly after acceptance, before technical editing, formatting and proof reading. Using this free service, authors can make their results available to the community, in citable form, before we publish the edited article. This *Accepted Manuscript* will be replaced by the edited, formatted and paginated article as soon as this is available.

You can find more information about *Accepted Manuscripts* in the **Information for Authors**.

RSC Advances Accepted Manuscript

Facile fabrication of the Cu@g-C₃N₄ nanocatalyst and its application for the aerobic oxidations of alkylaromatics and the reduction of 4-nitrophenol

Shen Huang, Yukai Zhao, Ruiren Tang*

School of Chemistry and Chemical Engineering, Central South University, Hunan, 410083, China

Corresponding author. Tel.: 86-731-88836961 Fax: 86-731-88879616

E-mail: trr@mail.csu.edu.cn

Abstract: In this study, the preparation of Cu@g-C₃N₄ nanocatalyst with highly-active sites was developed in a facile precipitation method by in situ reduction of Cu^{2+} adsorbed on the surface of layered graphitic carbon nitride (g-C₃N₄). The catalyst was characterized by FT-IR, XRD, SEM, TEM, ICP, XPS and BET, verifying that Cu nanoparticles with a mean particle size of 35.89 nm were uniformly distributed on the surface of g-C₃N₄. The reactions of alkylaromatics oxidation and 4-nitrophenol reduction were investigated on the Cu@g-C₃N₄ nanocatalyst with superior catalytic activity. The aerobic oxidation of ethylbenzene (EB) to acetophenone (AP) by *tert*-butyl hydroperoxide (TBHP) was conducted readily, and the conversion and selectivity could be reached to 98.8 % and 94.0 % under the optimal condition, respectively. Moreover, the reduction of 4-nitrophenol (4-NP) to 4-aminophenol (4-AP) employing NaBH₄ owns a the kinetic rate constant of 1.86×10^{-2} s^{-1} and an activity parameter of 1.134 $s^{-1} \cdot mM^{-1}$ in the presence of Cu@g-C₃N₄, which are higher than previous results described in the literatures.

Repeated cycles demonstrated the outstanding recyclability and stability of the catalyst for at least four runs without considerable loss of catalytic activity.

Key word: aerobic oxidation, catalytic reduction, g-C$_3$N$_4$, nanoparticles.

Introduction

Copper nanoparticles have opened great spirits in miscellaneous technological applications like optoelectronics, chemical sensing and catalysis owing to the properties of inexpensive, supernormal optical behaviors and easy accessibility. [1] Huang et al. [2] prepared Cu nanoparticle sensors and applied it to explore plasmon peak sensitivity. Du and coworkers [3] found that copper as a transparent electrocatalyst expanded application for water oxidation. In catalytic applications, a precise correlation between catalytic performance and particle size, however, the intractable problems that nanoparticles may be aggregated or grow during the reactions could lead to the decrease of the catalytic activity and further confine applications. [4] Therefore, dispersing metal particles on appropriate supporting materials with large surface areas have been applied to restrain the reunion of particles.

At present, graphitic carbon nitride (g-C$_3$N$_4$), an organic polymer semiconductor consisting mainly of carbon and nitrogen with band gap energy of 2.7 eV, has drawn extensive attention owing to large surface areas, particular physical features, high thermal stability, easily recycled, promising electronic and catalytic properties. [5, 6] It is formed by N-bridged tri-s-triazine repeating units which are generated by

two-dimensional conjugated planes packed together via van der Waals interactions. [7]

In view of its unique structure and preponderance, g-C_3N_4 has been widely employed

in various fields, for instance, oxygen reduction reaction, [8] water splitting, [9]

Suzuki-Miyaura coupling reaction, [10] bioimaging. [11] Up to now, Chen and coworkers

[12] empolyed g-C_3N_4 to catalyze oxidation of benzene to phenol. Su [13] reported aerobic

oxidative coupling of amines using g-C_3N_4 as photocatalyst. Nevertheless, the

catalytic property of g-C_3N_4 was limited due to low separation efficiency of

photogenerated electrone hole pairs and wide-band gap. [6] So strategies that depositing

nanoparticles onto g-C_3N_4 is regard as a convenient, straightforward, but effective

strategy to enhance the performance of g-C_3N_4.

Inspired by the unique architecture of g-C_3N_4 and the outstanding catalytic

performance of Cu nanoparticles, the g-C_3N_4 as support material judiciously

hybridized with copper nanoparticles to obtain a highly active and green

heterogeneous catalyst. More interestingly, the copper nanoparticles and g-C_3N_4 are

interdependent and mutually reinforcing. On the one hand, metal particles can

promote charge separation at the interface of the metal-semiconductor heterojunction,

which in turn lead to the improvement of catalytic performance. [14, 15] On the other

hand, the g-C_3N_4 as "active support" also can restrict the aggregation of metal

particles, thus further enhancing the selectivity and activity. [15] This enabled us to

explore the catalytic performance of Cu@g-C_3N_4 for alkylaromatics oxidation and

4-nitrophenol reduction. While the products of alkylaromatics oxidation as valuable

intermediates are pervasively applied in diversified areas like pharmaceuticals,

surfactants, agrochemicals and spice industry, [16-18] the transformation of 4-aminophenol (4-AP) by the catalytic hydrogenation of 4-nitrophenol (4-NP) is considered to be the most green, environmental, convenient way for the degradation of industrial effluents which contain mainly 4-NP without complicated composition. [19] The major challenge for the oxidation of alkylaromatics and the reduction of 4-nitrophenol concerns tedious workup procedures, poor activity, harsh conditions and the overuse of organic solvents in the presence of traditional catalysts. [20, 21] This demands the synthesis of novel catalysts to improve reaction properties. In this work, the nanocatalyst Cu@g-C$_3$N$_4$ was fabricated via a straight-forward chemical reduction method with ultra-high catalytic activity, and also can be reused without great loss of activity at least four runs.

2 Experimental

2.1 Materials

All chemicals were commercially available and were used without further purification. Deionized water was used throughout the experiments. Solvents were purified and dried according to standard methods. ICP were measured with Optima 5300DV, and the heterogeneous samples were preprocessed by acid digestion with concentrated nitric acid. FT-IR spectra were determined on a Nicolet NEXUS 670 FT-IR spectrophotometer using KBr discs in the 400–4000 cm^{-1} region under atmospheric conditions. The products of oxidation reactions were monitored using Techcomp GC-7890II gas chromatograph with a OV-1701 column (50 m × 0.25 mm × 0.25 μm) and flame ionization detector (FID). Scanning electron microscopy (SEM) were

examined by FEI QUANTA 200 microscope. Transmission Electron Microscope (TEM) images were recorded with a JEOL JEM-2100F microscope. The ultraviolet visible spectra (UV–Vis) were conducted by Shimadzu UV-2600. N_2 gas adsorption and desorption analyses were taken using Quantachrome instruments, BoyntonBeach, FL33426 at constant temperature (-196 ^{o}C). The power X-ray diffraction (XRD) patterns were conducted using a Rigaku D/Max III VC diffractometer in the range of $2\theta = 10$–80°. X-ray photoelectron spectroscopy (XPS) measurements were characterized by ThermoFisher-VG Scientific ESCALAB 250Xi. ^{1}H NMR measurement were performed on a Bruker-400 MHz nuclear magnetic resonance spectrometer with deuterated chloroform as solvent and TMS as internal reference.

2.2 Synthesis of Cu@g-C_3N_4 Catalyst

The support g-C_3N_4 was prepared through the heat polymerization of melamine on the basis of the previously reported methods. [5, 22] Typically, melamine was put into a ceramic crucible with a cover and placed into the muffle furnace, heated at a rate of 3 ^{o}C/min until the temperature up to 550 ^{o}C, and kept at this temperature for 4 h. When cooling to room temperature, the primrose yellow polymer was milled to obtain g-C_3N_4 powder. The Cu@g-C_3N_4 was synthesized by a facile precipitation method. [6] As described below: 500 mg of as-prepared g-C_3N_4 was dispersed in 100 mL deionized water to obtain the uniformity of dispersion by ultrasonic method. Then 10 mL $CuCl_2$ (84 mg) aqueous solution was added dropwise under strong stirring. The mixed solutions was stirred at room temperature for 10 h. 1 M NaOH aqueous solution was added dropwise until the pH of mixture was approximately equal to 10.

After an hour, 30 mL NaBH$_4$ (1 M) aqueous solution was added to reduce Cu (II) to Cu (0). The greyish-green precipitate was filtrated, washed with deionized water (3×25 mL) and alcohol (3×25 mL), and dried under vacuum at 70 ^{o}C for 8 h.

2.3 Typical Procedure for ethylbenzene oxidation

The oxidation of ethylbenzene was chosen as a model reaction. Reactions were conducted by suspending the Cu@g-C$_3$N$_4$ catalyst in a acetonitrile solution (10 mL) containing ethylbenzene (10 mmol). The catalyst was stirred and swollen. Then TBHP (a number of 70% aqueous solution) was added dropwise, and the mixture was stirred at a certain temperature for the required time. After the reaction finished, the catalyst was filtrated, washed with acetonitrile and 1 M NaOH solution. The saturated aqueous NaHSO$_3$ solution was added into the filter liquor to remove the extra TBHP. The filtrate was extracted with ethyl acetate (3×10 mL). The organic phase was washed with saturated aqueous EDTA solution, saturated NaHCO$_3$ solution, deionised water and dried over anhydrous Na$_2$SO$_4$.The products in reactions were analyzed by GC.

2.4 Typical Procedure for the Reduction of 4-nitrophenol

In a typical reaction, 2.8 mL deionized water and 40 μL 4-NP (0.01 M) were mixed to a colorimetric ware, following 80 μL freshly prepared NaBH$_4$ solution (0.5 M) was added, resulting in the appearance of a bright yellow solution. After that, 10 μL Cu@g-C$_3$N$_4$ catalyst (5 mg/mL) was added to the above mixed solution, and the color of solution faded from bright yellow to colorless slowly. The reaction conversion was monitored by ultraviolet visible spectra (UV–Vis).

2.5 Catalyst Recycling Test

The recovery of the Cu@g-C$_3$N$_4$ catalyst for the oxidation of ethylbenzene (EB) is represented below. EB (10 mmol), TBHP (50 mmol), acetonitrile (10 mL) and Cu@g-C$_3$N$_4$ (80 mg) were mixed into a 50 mL round bottomed flask. The mixture was stirred at 80 ^{o}C for 6 h. At the end of the reaction, the catalyst was separated by filtration and washed with acetonitrile and 1 M NaOH solution, dried under vacuum at 50 ^{o}C. The obtained catalyst was used for the next cycles.

3 Results and Discussion

3.1 Characterization of catalyst

3.1.1 Fourier Transform Infrared

The FT-IR spectra of g-C$_3$N$_4$ and Cu@g-C$_3$N$_4$ are shown in Figure 1. It is clear that the sharp peak at 806 cm^{-1} comes from out-of plane bending vibration of triazine cycle. The peak at 1645 cm^{-1} was referred to heterocyclic C=N stretching vibration, while the peak at 1238, 1317, 1405 and 1543 cm^{-1} were considered as C–N stretching of tri-s-triazine. The broad bands ranging from 2800 to 3400 cm^{-1} assigning to N-H (uncondensed terminal amino groups) stretching vibration were observed in g-C$_3$N$_4$.[23] After Cu was loaded, almost nothing has essentially changed in the FT-IR spectrum, making clear that there was no covalent-bond interaction between g-C$_3$N$_4$ and Cu nanoparticles.
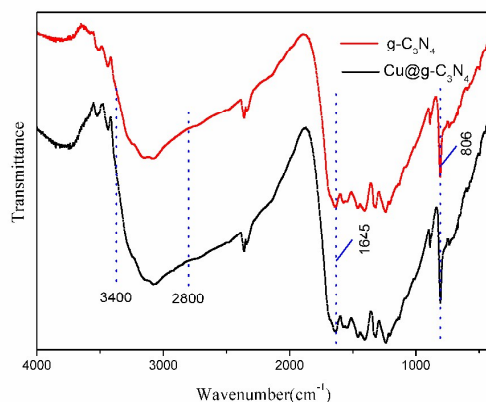
Fig. 1 FT-IR spectra of g-C$_3$N$_4$ and Cu@g-C$_3$N$_4$

3.1.2 X-ray diffraction

The X-ray diffraction (XRD) patterns of pure g-C$_3$N$_4$ and Cu@g-C$_3$N$_4$ were performed in Figure 2. The sharp and strong peak at 27.5° was observed in pure g-C$_3$N$_4$, corresponding to the characteristic (002) interlayer stacking peak of g-C$_3$N$_4$.[24] The (100) weak diffraction peak at 13.1° was attributed to the in-plane repeated units in the g-C$_3$N$_4$.[25] After loading Cu, the intensity peak at 27.5° decreased mildly as a result of dilution effect.[6] Moreover, new typical peaks appeared in the XRD pattern of Cu@g-C$_3$N$_4$. The (111), (200), (220) another diffraction peaks located at 43.3°, 50.4° and 74.1° represented the planes of the face centered cubic Cu,[24] suggesting that as-prepared sample takes on a two-phase composition.
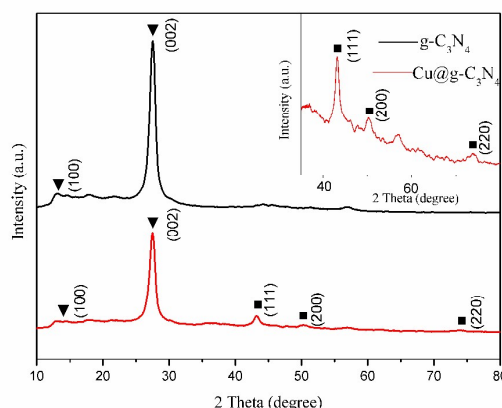
Fig. 2 XRD patterns of pure C_3N_4 and Cu@g-C_3N_4

3.1.3 X-ray photoelectron spectroscopy

The X-ray photoelectron spectroscopy (XPS) of Cu@g-C_3N_4 was shown in Figure 3. The coexistence of elements C, N, O and Cu in the Cu@g-C_3N_4 catalyst were observed from the survey spectrum. The C 1s signal could be identified with two main peaks at binding energies of 284.8 and 288.3 eV, which corresponded to sp^2 carbon (C−C) and sp^2-bonded carbon (N−C=N), respectively. [26] The three main N 1s peaks were exhibited at 398.8, 400.1 and 401.3 eV, which assigned to sp^2-hybridized nitrogen (C=N−C), sp^3-hybridized nitrogen tertiary nitrogen (N-(C)$_3$), and amino functional groups with one hydrogen atom (C−N−H) respectively. [27] The peaks located at 935.3 and 955.2 eV attributed to Cu^{2+} species $2p_{3/2}$ and $2p_{1/2}$. Meanwhile, two shake-up lines centered at 944.1 and 963.0 eV are measured, meaning the existence of paramagnetic chemical state of Cu^{2+}. [28] Indeed, the binding energies of Cu $2p_{3/2}$ and Cu $2p_{1/2}$ shift to 932.7 and 952.7 eV, respectively, indicating the formation of metal Cu. [6] The Cu(0)/Cu(II) ratio was calculated as 1.869, suggesting that Cu(II) can be partially reduce to Cu(0) and Cu(0) takes up a majority.
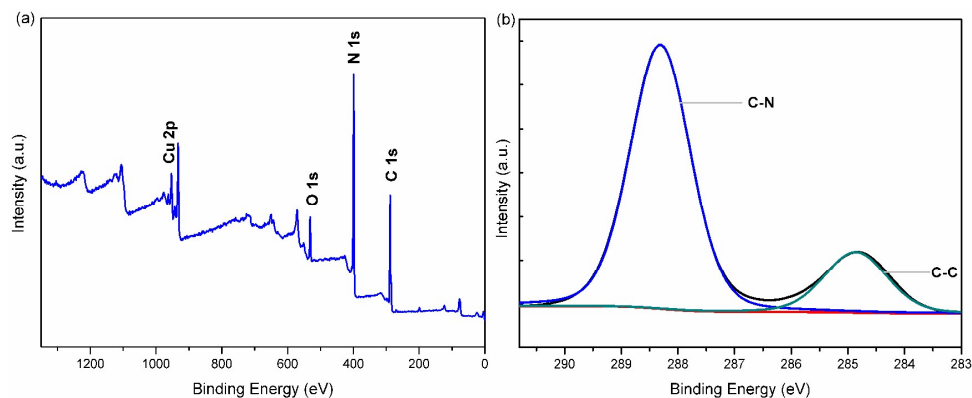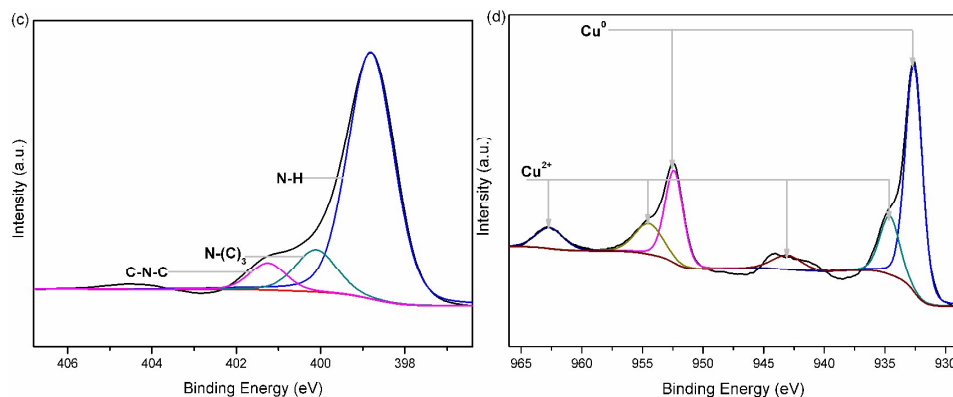
Fig. 3 The XPS spectrum of Cu@g-C_3N_4: (a) survey, (b) C 1s, (c) N 1s and (d) Cu 2p

3.1.4 Surface area and porosity measurements

The surface area and porous architecture of the g-C_3N_4 support and the as-made

Cu@g-C_3N_4 catalyst were measured. As you can see in Figure 4, the surface area and

pore size of g-C_3N_4 were calculated to be 10.015 m^2/g and 3.816 nm, respectively.

Clearly, the g-C_3N_4 has a type IV adsorption−desorption isotherms, which conforming

the representative mesoporous structure. [29] There was no significant change in the

isotherm profile and the pore diameter for Cu@g-C_3N_4, suggesting that the Cu

nanoparticles did not break the pore distribution, which is in accordance with the

presence of the plane structure after the loading of Cu nanoparticles. In addition, the

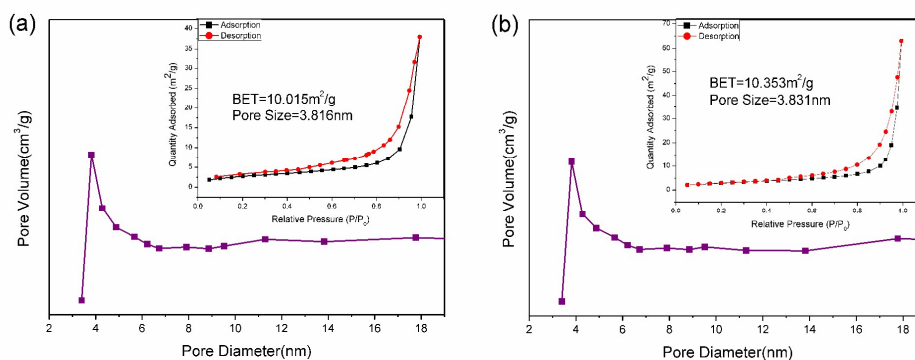content of Cu in the Cu@g-C_3N_4 is determined to be 6.34% by ICP-AES.

Fig. 4 N_2 adsorption−desorption isotherms and the corresponding pore-size distribution curves of

(a) g-C$_3$N$_4$ and (b) Cu@g-C$_3$N$_4$.

3.1.5 Scanning Electron Microscope (SEM) and Transmission Electron Microscope (TEM)

The SEM and TEM images of g-C$_3$N$_4$ and Cu@g-C$_3$N$_4$ are shown in Figure 5. The g-C$_3$N$_4$ possesses a typical stacked layered structure, resulting in porous morphology. It is clear that the shape of g-C$_3$N$_4$ was not broken after the introduction of Cu nanoparticles, verifying the Cu nanoparticles was sedimented on the surface of g-C$_3$N$_4$. The TEM image (Figure 5e) of Cu@g-C$_3$N$_4$ exhibited that Cu nanoparticles were dispersed homogeneously on the surface of the g-C$_3$N$_4$ with an average particle size of 35.89 nm, which is in good consistent with the results of XRD and XPS. Moreover, the morphology of Cu@g-C$_3$N$_4$ remained unchanged after recycling, which reflects that the Cu@g-C$_3$N$_4$ designed and prepared in our research was stable and robust.
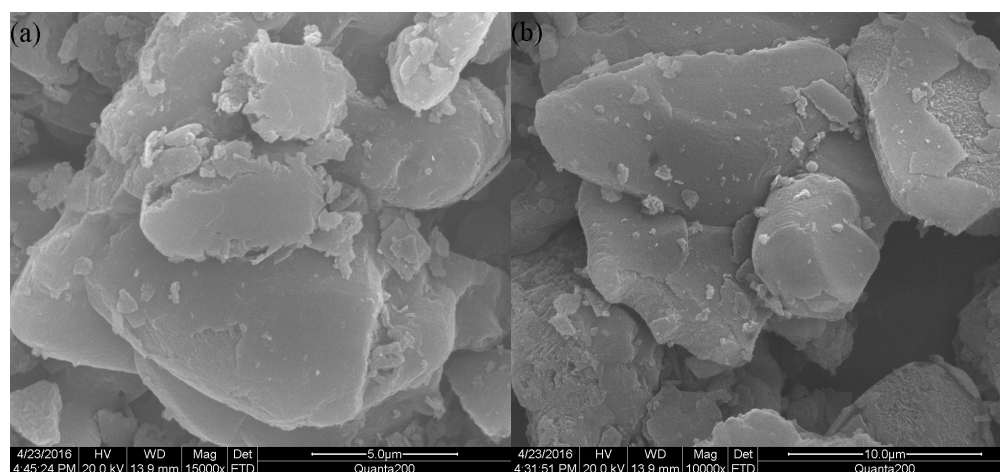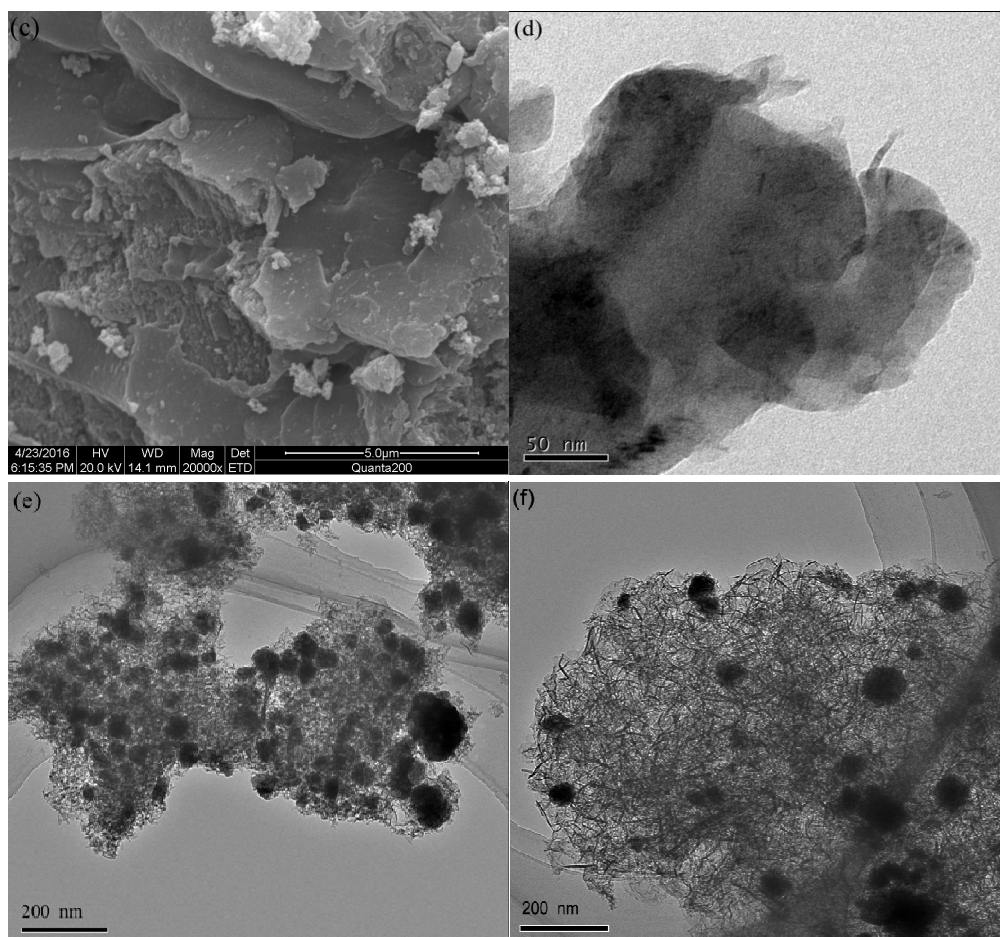
Fig. 5 SEM images of (a) g-C$_3$N$_4$, (b) the fresh Cu@g-C$_3$N$_4$ and (c) the reused Cu@g-C$_3$N$_4$. TEM

images of (d) g-C$_3$N$_4$, (e) the fresh Cu@g-C$_3$N$_4$ and (f) the reused Cu@g-C$_3$N$_4$.

3.2 Effect of different reaction conditions for oxidation of ethylbenzene

3.2.1 Effect of catalyst amount

As shown in Table 1, the conversion of EB oxidation was extremely low in the

absence of catalyst. When the introduction of Cu@g-C$_3$N$_4$, and discovered that the

EB conversion and the AP selectivity both improved markedly. It should be noted that

with 80 mg Cu@g-C$_3$N$_4$ conversion reached a maximum. The EB conversion

decreases slightly with the further increase of catalyst, and the reason is that the

carbon or coke deposition at excess catalyst concentrations probably impede the

active sites of the catalysts. And the AP selectivity increased within a narrow range
with increasing catalyst amount. In view of practical application, 80 mg Cu@g-C$_3$N$_4$
was chosen as the suitable catalyst amount.

Table 1 Effect of catalyst amount for the oxidation of EB

Entry	Catalyst	Catalyst amount (mg)	Con. (%)	Sel. (%)	
				AP	BAL
1	Cu@g-C$_3$N$_4$	0	16.7	67.6	32.4
2	Cu@g-C$_3$N$_4$	20	83.9	85.7	14.3
3	Cu@g-C$_3$N$_4$	40	84.1	87.2	12.8
4	Cu@g-C$_3$N$_4$	60	87.7	87.9	12.1
5	Cu@g-C$_3$N$_4$	80	92.8	88.5	11.5
6	Cu@g-C$_3$N$_4$	100	90.4	88.7	11.3
7	g-C$_3$N$_4$	80	43.8	60.2	39.8

Conditions: 10 mmol ethylbenzene (EB), different amount of Cu@g-C$_3$N$_4$, 5 equiv of 70 % TBHP
in CH$_3$CN (10 mL) were stirred at 80 ^{o}C for 4 h. AP = acetophenone, BAL = benzaldehyde.

3.2.2 Effect of reaction temperature

Further experiments were performed to explore the effect of reaction temperature.
From Table 2, both the conversion of EB and the selectivity of AP went up with
increase of reaction temperature. The maximum conversion (92.8 %) and selectivity
(88.5 %) was observed at 80 ^{o}C and then lower slightly at higher temperature. Hence,
80 ^{o}C was used as the optimal temperature in the following reactions.

Table 2 Effect of reaction temperature for the oxidation of EB

RSC Advances Accepted Manuscript

Entry	Temperature (^{o}C)	Con. (%)	Sel. (%)	
			AP	BAL
1	50	71.9	84.0	16.0
2	60	78.5	84.6	15.4
3	70	88.7	87.4	12.6
4	80	92.8	88.5	11.5
5	90	86.2	79.5	20.5

Conditions: 10 mmol ethylbenzene (EB), 80 mg Cu@g-C$_3$N$_4$, 5 equiv of 70 % TBHP in CH$_3$CN

(10 mL) were stirred for 4 h within several temperature. AP = acetophenone, BAL =

benzaldehyde.

3.2.3 Effect of Reaction Time

The following researches under the optimizations mentioned above were carried out

to determine the ideal reaction time. As illustrated, the conversion of EB and the

selectivity of AP increased with prolonging time from 2 to 6 h, then the conversion

dropped slightly in the longer reaction time. Therefore, 6 h was chosen to keep better

efficiency for the conversion, selectivity and reaction time.

Table 3 Effect of reaction time for the oxidation of EB

Entry	Reaction time (h)	Con. (%)	Sel. (%)	
			AP	BAL
1	2	91.3	85.6	14.4
2	4	92.8	88.5	11.5
3	6	97.1	89.2	10.8

4	8	91.6	90.5	9.5
5	10	89.2	89.4	10.6

Conditions: 10 mmol ethylbenzene (EB), 80 mg Cu@g-C_3N_4, 5 equiv of 70 % TBHP in CH_3CN (10 mL) were stirred at 80 ^{o}C within several time. AP = acetophenone, BAL = benzaldehyde.

3.2.4 Effect of TBHP amount

Subsequently, tests were conducted using different molar equivalents of TBHP in order to get an optimized value. As expected, the EB conversion improved remarkably from 57.3 to 97.1 % with increasing TBHP amount from 10 to 50 mmol, while it changed very slightly in a higher concentration (60 mmol) of TBHP. It is a reason that at lower TBHP concentration, insufficient TBHP could be activated by catalyst, the oxidation of EB is difficult. Excessive oxidizing agent has no significant effect to aerobic oxidation when TBHP reaches saturation. The change rule of the AP selectivity in accordance with the EB conversion. In view of practical application, 50 mmol TBHP was selected as the best amount for the reactions involved in.

Table 4 Effect of TBHP amount for the oxidation of EB

Entry	TBHP amount (mmol)	Con. (%)	Sel. (%)	
			AP	BAL
1	10	57.3	71.8	28.2
2	20	70.3	75.6	24.4
3	30	70.8	83.4	16.6
4	40	77.9	84.9	15.1
5	50	97.1	89.2	10.8

| 6 | 60 | 97.3 | 89.9 | 11.1 |

Conditions: 10 mmol ethylbenzene (EB), 80 mg Cu@g-C$_3$N$_4$, different equiv of 70 % TBHP in CH$_3$CN (10 mL) were stirred at 80 ^{o}C for 6 h. AP = acetophenone, BAL = benzaldehyde.

3.2.5 Effect of different co-catalysts

Some co-catalysts were added to reaction mixture in order to further promote the catalytic activity. As the Table 5 listed, *N*-hydroxyphthalimide (NHPI) could improve markedly the EB conversion and the AP selectivity compared with Cu@g-C$_3$N$_4$ as the sole catalyst. This fact can be explained for the following reasons: the oxidation of EB is likely to follow the free radical chain mechanism, and NHPI as electron transfer initiates the radical propagation of autoxidation via one electron transfer and enhances the catalytic activity. Conversely, the conversion and selectivity actually lowered in presence of other co-catalysts. The different activation mechanisms of the co-catalysts may be the reason. Accordingly, NHPI should be the suitable co-catalyst.

Table 5 Effect of co-catalysts for the oxidation of EB

Entry	Co-catalysts	Con. (%)	Sel. (%)	
			AP	BAL
1	NHPI	98.8	94.0	6.0
2	AIBN	87.3	77.1	22.9
3	CTAB	73.0	68.3	31.7
4	TBAB	65.1	72.8	27.2

Conditions: 10 mmol ethylbenzene (EB), 80 mg Cu@g-C$_3$N$_4$, 5 equiv of 70 % TBHP, 1 mmol different co-catalyst in CH$_3$CN (10 mL) were stirred at 80 ^{o}C for 6 h. AP = acetophenone, BAL =

benzaldehyde, AIBN = α,α'-azobisisobutyronitrile, CTAB = hexadecyl trimethyl ammonium bromide, TBAB = tetrabutyl ammonium bromide.

3.2.6 Reused of the Cu@g-C_3N_4 catalyst

The stability and reuse of catalyst play a critical role in heterogeneous catalytic reactions. Further studies were proceeded to examine the recyclability of Cu@g-C_3N_4. It was clearly seen that, the EB conversion and the AP selectivity decreased marginally in the second time and changed very slightly after that. The catalytic activity of Cu@g-C_3N_4 was well retained after 4 runs (the conversion of EB > 93 % and the selectivity of AP > 84 %). Moreover, the color, FT-IR spectra, SEM, TEM, morphology have no obvious change, indicating that the catalyst Cu@g-C_3N_4 was stable and robust.

Table 6 The reusability of the Cu@g-C_3N_4 catalyst for the oxidation of EB

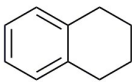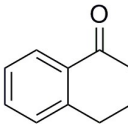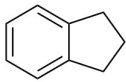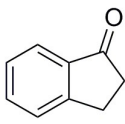| Entry	Cycle No.	Con. (%)	Sel. (%)	
			AP	BAL
1	Fresh	97.1	89.2	10.8
2	1	94.4	85.5	14.5
3	2	93.7	85.2	14.8
4	3	93.1	84.8	15.2
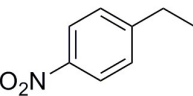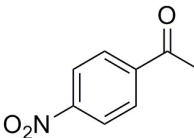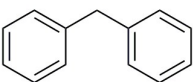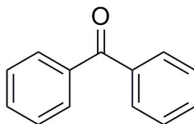
Conditions: 10 mmol ethylbenzene (EB), 80 mg Cu@g-C_3N_4 of different cycles times, 5 equiv of 70 % TBHP in CH_3CN (10 mL) were stirred at 80 °C for 6 h. AP = acetophenone, BAL = benzaldehyde.
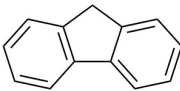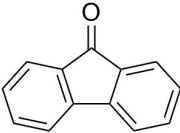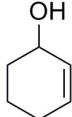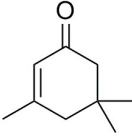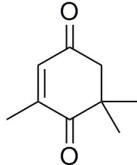
3.2.7 Oxidation of different substrates catalyzed by Cu@g-C_3N_4

A series of substrates were used to investigate the generality of catalytic performance

of as-made Cu@g-C$_3$N$_4$ under the optimal conditions in Table 7. The reactions

processed smoothly in acetonitrile as the solvent and using TBHP as the oxidizing

agent afforded the desired oxidative products in outstanding conversion (90-100%)

but α-isophorone (the conversion was 55.8 %), with selectivities ranging from 80 to

98 % , confirming a very good catalytic activity. The groups containing either an

electron-attracting or an electron-donating group in the aromatic ring did not seem to

have distinct influence on the reaction results for aromatic substrate. Moreover,

cyclohexene was oxidized with 2-cyclohexen-1-ol as main product, giving completely

conversion and the selectivity of 83.4 %. In sharp contrast, low α-isophorone

conversion (55.8 %) was achieved with moderate selectivity for product

ketoisophorone (80.1 %).

Table 7 Oxidation of different substrates catalyzed by Cu@g-C$_3$N$_4$ catalyst

Entry	Substrate	Main product	Con. (%)	Sel. (%)
1			90.1	95.8
2			94.4	97.2
3			95.6	97.7
4			95.1	93.6

5			93.9	98.5
6			100	83.4
7			55.8	80.1

Conditions: 10 mmol substrate, 80 mg Cu@g-C$_3$N$_4$, 5 equiv of 70 % TBHP in CH$_3$CN (10 mL) were stirred at 80 $^{\circ}$C for 6 h. The characterization of the products by ^{1}H NMR and the spectra were shown in supporting information.

3.2.8 Possible reaction mechanism for EB oxidation

Based on the experimental results and related published literatrues, [30-32] the proposed reaction mechanism for EB oxidation is thought to proceed via a radical-chain sequence mechanism and shown in Scheme 1. It can be surmised that firstly TBHP was adsorbed onto the surface of the Cu@g-C$_3$N$_4$ because of its large surface area, sequentially O-O bond in TBHP broken to form *tert*-butyl oxygen and hydroxyl radicals due to Cu^{2+} could activate the lone pair of electrons of the distant oxygen in TBHP. The above radicals can capture the α-H of EB to generate α-ethylbenzene radical. Synchronously, the α-ethylbenzene radical is captured by TBHP producing *tert*-butylperoxy ethers. At last, AP as main product and BAL as by-product can be formed by two ways.
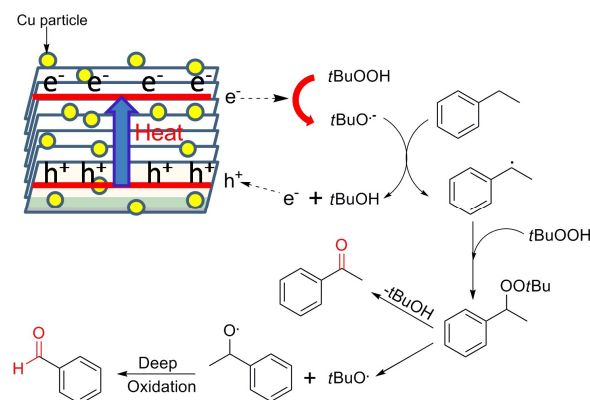
Scheme 1 Possible reaction mechanism

3.3 Cu@g-C$_3$N$_4$ for Reduction of 4-nitrophenol

The catalytic performance of Cu@g-C$_3$N$_4$ was assessed using the reduction of 4-nitrophenol (4-NP) into 4-aminophenol (4-AP) in the presence of excess NaBH$_4$. The process of this reaction was monitored by measuring the UV-Vis absorption intensity. Figure 6 shows the characteristic peak of 4-nitrophenol shifts from 317 to 400 nm after the addition of NaBH$_4$ solution, accompanying with the color changes from colorless to bright yellow due to the forming of 4-nitrophenolate. [33] The spectral profile at 400 nm remained constant even after 10 h in the lack of a catalyst, [34] because the reaction is kinetically restricted but thermodynamically feasible. Whereas, when the introduction of Cu@g-C$_3$N$_4$, the intensity of the peak at 400 nm decreased progressively to be disappeared in 360 seconds with the bleaching of the bright yellow color of the reaction solution. Simultaneously, a new peak assigning to the typical absorption of 4-AP increased gradually.

RSC Advances Accepted Manuscript
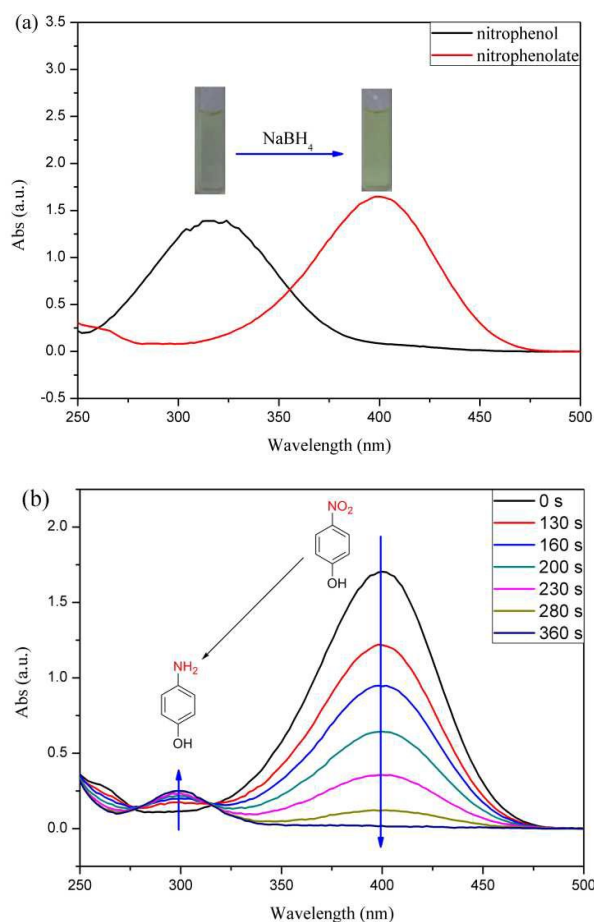
Figure 6. (a) UV–Vis spectra of 4-NP before and after addition of NaBH$_4$ solution. (b) The

reduction process of 4-NP to 4-AP in the presence of Cu@g-C$_3$N$_4$ catalyst.

The concentration of NaBH$_4$ was very high in comparison to that of 4-NP and thus the

reaction process followed pseudo-first-order reaction kinetics. [35] Therefore,

pseudo-first-order kinetics was used to measure the kinetic rate constant (k_{app}) and the

activity parameter (k) of Cu@g-C$_3$N$_4$. We calculated the reaction conversion from

C_t/C_0 (Figure 7), which was determined using the relative intensity of the UV-Vis

absorbance (A_t/A_0) at 400 nm. C_t and C_0 are the concentrations of the 4-NP at reaction

time t and the initial stage, respectively.

$$\ln(C_t/C_0) = \ln(A_t/A_0) = -k_{app} t \qquad (1)$$

$$k = k_{app} / c_{(Cu)} \qquad\qquad (2)$$

The kinetic rate constant (k_{app}) was calculated to be 1.86×10^{-2} s^{-1} in reduction of 4-NP using Cu@g-C$_3$N$_4$ as catalyst. The activity parameter (k) was designated by normalizing to the concentration of Cu and the result of k is 1.134 s^{-1}·mM^{-1}, suggesting that Cu@g-C$_3$N$_4$ was excellent catalytic activity for 4-NP reduction.
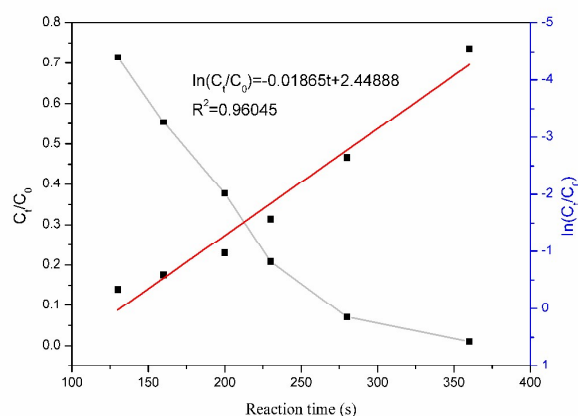
Figure 7. Plots of C_t/C_0 and $\ln(C_t/C_0)$ versus reaction time for the reduction of 4-NP in the presence of Cu@g-C$_3$N$_4$ catalyst.

In addition, we further compared the catalytic activity of the Cu@g-C$_3$N$_4$ with other catalysts that reported in the reduction of 4-NP. As shown in Table 8, the Cu@g-C$_3$N$_4$ catalyst performed the best with the active parameter k as 1.134 s^{-1}·mM^{-1}.

Table 8 Comparison of the apparent kinetic rate constant (k_{app}) and activity parameter

(k) of different catalysts for the reduction of 4-NP

Samples	$c_{(4\text{-NP})}$[a] (mM)	$c_{(M)}$[a] (mM)	k_{app}[b] (s^{-1})	k[c] (s^{-1}·mM^{-1})	Number of cycle	activation energy (kJ·mol^{-1})	Ref.
CuFe$_2$O$_4$	0.17	1.56×10^{-1}	1.2×10^{-1}	0.769	2	-	34

RSC Advances Accepted Manuscript

	c^a		k$_{app}$^{b}			k^c	
nanoparticles							
Pd nanoclusters	0.2	1.6	7.89×10^{-4}	0.0005	-	-	[36]
Pd/PiHP	2.3	9×10^{-2}	20×10^{-3}	0.222	6	-	[37]
Pd/FG	5.8×10^{-2}	4.72×10^{-3}	2.35×10^{-3}	0.498	5	-	[33]
p(SPM)-Cu composite	10	2.8	4.24×10^{-3}	1.5×10^{-3}	7	33.86	[38]
p(AAGA)-Ag	10	2.148	1.52×10^{-3}	7.1×10^{-3}	5	33.78	[39]
p(MAc)-Cu composite	10	6.77×10^{-2}	2.41×10^{-2}	0.3556	4	31.33	[40]
p(TA)-Co composite ILs	10	1.475×10^{-2}	7.167×10^{-3}	0.4859	5	26.19	[41]
p(AMPS)-Cu	15	3.437×10^{-1}	1.72×10^{-3}	0.005	5	28.16	[42]
Cu@g-C$_3$N$_4$	0.13	1.64×10^{-2}	1.86×10^{-2}	1.134	4	-	This work

^{a}c: concentration. ^{b}k$_{app}$: pseudo-first-order rate constant. ^{c}k: catalytic parameter. Data were given or calculated in the respective papers.

4 Conclusion

In this study, we described the preparation and characterization of Cu@g-C$_3$N$_4$ nanocatalyst, which enabled us to explore its applications in the oxidation of alkylaromatics and the reduction of 4-nitrophenol. The Cu@g-C$_3$N$_4$ exhibited excellent catalytic performance for the oxidation of ethylbenzene with 98.8 % conversion and 94.0 % selectivity, and the active parameter k as 1.134 s^{-1}·mM^{-1} for

the reduction of 4-nitrophenol. Furthermore, the as-prepared catalyst could be recovered and reused by filtration without considerable loss of catalytic activity, indicating that Cu@g-C$_3$N$_4$ as an efficient, economic and environmental heterogenous catalyst could provide new insights for green chemistry and industrial applications.

References

1.   J. Qiu, N. E. Richey, J. S. DuChene, Y. Zhai, Y. Zhang, L. McElwee-White and W. D. Wei, *The Journal of Physical Chemistry C*, 2016.

2.   M. Huang, Y. Zhang, C. Du, S. Peng and D. Shi, *Plasmonics*, 2016, 1-4.

3.   J. L. Du, Z. F. Chen, S. R. Ye, B. J. Wiley and T. J. Meyer, *Angewandte Chemie-International Edition*, 2015, 54, 2073-2078.

4.   Z. A. Qiao, P. F. Zhang, S. H. Chai, M. F. Chi, G. M. Veith, N. C. Gallego, M. Kidder and S. Dai, *J. Am. Chem. Soc.*, 2014, 136, 11260-11263.

5.   G. Y. Liu, R. R. Tang and Z. Wang, *Catal. Lett.*, 2014, 144, 717-722.

6.   X. S. Zhou, Z. H. Luo, P. F. Tao, B. Jin, Z. J. Wu and Y. S. Huang, *Mater. Chem. Phys.*, 2014, 143, 1462-1468.

7.   H.-B. Fang, Y. Luo, Y.-Z. Zheng, W. Ma and X. Tao, *Industrial & Engineering Chemistry Research*, 2016.

8.   H. Li, Y. Liu, X. Gao, C. Fu and X. Wang, *ChemSusChem*, 2015, 8, 1189-1196.

9.   Z. Li, C. Kong and G. Lu, *The Journal of Physical Chemistry C*, 2015, 120, 56-63.

10.   J. Sun, Y. Fu, G. He, X. Sun and X. Wang, *Applied Catalysis B: Environmental*, 2015, 165, 661-667.

RSC Advances Accepted Manuscript

11.   Y. Wang, X. C. Wang and M. Antonietti, *Angewandte Chemie-International Edition*, 2012, 51, 68-89.

12.   X. F. Chen, J. S. Zhang, X. Z. Fu, M. Antonietti and X. C. Wang, *J. Am. Chem. Soc.*, 2009, 131, 11658-+.

13.   F. Z. Su, S. C. Mathew, L. Mohlmann, M. Antonietti, X. C. Wang and S. Blechert, *Angewandte Chemie-International Edition*, 2011, 50, 657-660.

14.   X.-H. Li and M. Antonietti, *Chem. Soc. Rev.*, 2013, 42, 6593-6604.

15.   Y. Gong, M. Li, H. Li and Y. Wang, *Green Chemistry*, 2015, 17, 715-736.

16.   K. X. Chen, P. F. Zhang, Y. Wang and H. R. Li, *Green Chemistry*, 2014, 16, 2344-2374.

17.   G. Zou, D. Jing, W. Zhong, F. Zhao, L. Mao, Q. Xu, J. Xiao and D. Yin, *RSC Advances*, 2016, 6, 3729-3734.

18.   Y. Qi, Y. Luan, J. Yu, X. Peng and G. Wang, *Chemistry–A European Journal*, 2015, 21, 1589-1597.

19.   Y. C. Chang and D. H. Chen, *J. Hazard. Mater.*, 2009, 165, 664-669.

20.   A. Wusiman and C. D. Lu, *Appl. Organomet. Chem.*, 2015, 29, 254-258.

21.   J. R. Chiou, B. H. Lai, K. C. Hsu and D. H. Chen, *J. Hazard. Mater.*, 2013, 248, 394-400.

22.   Y. K. Zhao, R. R. Tang and R. Huang, *Catal. Lett.*, 2015, 145, 1961-1971.

23.   J. Q. Yan, H. Wu, H. Chen, L. Q. Pang, Y. X. Zhang, R. B. Jiang, L. D. Li and S. Z. Liu, *Applied Catalysis B-Environmental*, 2016, 194, 74-83.

24.   J. Yang, H. T. Zhang, B. B. Chen, H. Tang, C. S. Lia and Z. Z. Zhang, *Rsc Advances*, 2015, 5, 64254-64260.

25.   X. X. Zou, R. Silva, A. Goswami and T. Asefa, *Appl. Surf. Sci.*, 2015, 357, 221-228.

26.   T. Xiong, W. Cen, Y. Zhang and F. Dong, *ACS Catalysis*, 2016, 6, 2462-2472.

27.   C. Ye, J.-X. Li, Z.-J. Li, X.-B. Li, X.-B. Fan, L.-P. Zhang, B. Chen, C.-H. Tung and L.-Z. Wu, *ACS Catalysis*, 2015, 5, 6973-6979.

28.   J. Yu and J. Ran, *Energy & Environmental Science*, 2011, 4, 1364-1371.

29.   F. Dong, Z. W. Zhao, T. Xiong, Z. L. Ni, W. D. Zhang, Y. J. Sun and W. K. Ho, *Acs Applied Materials & Interfaces*, 2013, 5, 11392-11401.

30.   R. F. Xie, G. L. Fan, L. Yang and F. Li, *Chem. Eng. J.*, 2016, 288, 169-178.

31.   T. Liu, H. Y. Cheng, L. S. Sun, F. Liang, C. Zhang, Z. Ying, W. W. Lin and F. Y. Zhao, *Applied Catalysis a-General*, 2016, 512, 9-14.

32.   M. Arshadi, M. Ghiaci, A. Rahmanian, H. Ghaziaskar and A. Gil, *Applied Catalysis B-Environmental*, 2012, 119, 81-90.

33.   Z. M. Wang, C. L. Xu, G. Q. Gao and X. Li, *Rsc Advances*, 2014, 4, 13644-13651.

34.   J. Feng, L. Su, Y. H. Ma, C. L. Ren, Q. Guo and X. G. Chen, *Chem. Eng. J.*, 2013, 221, 16-24.

35.   Z. P. Dong, X. D. Le, X. L. Li, W. Zhang, C. X. Dong and J. T. Ma, *Applied Catalysis B-Environmental*, 2014, 158, 129-135.

36.   A. Halder, S. Patra, B. Viswanath, N. Munichandraiah and N. Ravishankar, *Nanoscale*, 2011, 3, 725-730.

37.   H. Li, L. Han, J. Cooper-White and I. Kim, *Green Chemistry*, 2012, 14, 586-591.

38.   N. Sahiner, A. Kaynak and S. Butun, *J. Non-Cryst. Solids*, 2012, 358, 758-764.

39.   S. Butun and N. Sahiner, *Polymer*, 2011, 52, 4834-4840.

40.   M. Ajmal, M. Siddiq, H. Al-Lohedan and N. Sahiner, *Rsc Advances*, 2014, 4, 59562-59570.

41.   N. Sahiner, S. Sagbas and N. Aktas, *Rsc Advances*, 2015, 5, 18183-18195.

42.   N. Sahiner and O. Ozay, *Current Nanoscience*, 2012, 8, 367-374.

Graphical Abstract

Con.$_{max}$ = 98.8 %
Sel.$_{max}$ = 94.0 %

k = 1.134 s^{-1}·mM^{-1}